Journal of the Korean Physical Society, Vol. 55, No. 4, October 2009, pp. 1472∼1477

Photocatalytic Hydrogen Generation from Water-methanol Mixtures Using Nanocrystalline $ZnFe_2O_4$ under Visible Light Irradiation

P. H. Borse
Center for Nanomaterials, International Advanced Research Center for Powder Metallurgy and New Materials (ARC International), Balapur PO, Hyderabad, AP, 500-005, India

J. S. Jang, S. J. Hong and J. S. Lee
Department of Chemical Engineering, Pohang University of Science and Technology, Pohang 790-784

J. H. Jung
Division of Biotechnology and Health, Sorabol College

T. E. Hong, C. W. Ahn, E. D. Jeong, K. S. Hong, J. H. Yoon and H. G. Kim*
Busan Center, Korea Basic Science Institute, Busan 609-735

(Received 2 June 2009)

A spinel crystal structure of ferrite containing zinc ($ZnFe_2O_4$) was synthesized by using the polymer complex method. A pure phase $ZnFe_2O_4$ was obtained at a relatively lower temperature of 900 °C. The as-synthesized nanoparticles are agglomerates of crystals with an average size of ∼50 nm, as estimated from the X-ray diffraction analysis. The band gap of the *n*-type semiconducting metal oxide, as determined by using an ultraviolet-visible diffuse reflectance spectrometer was found to be 1.90 eV (653 nm). The photocatalytic activity of $ZnFe_2O_4$ was investigated by using the photoreduction of water under visible light (≥420 nm), which was found to be much higher than that of the well-known $TiO_{2-x}N_x$ photocatalyst. This superior performance is attributed to the larger surface area, the uniform and well-dispersed deposition of the Pt co-catalyst over the surface, and the small band gap of the chemically-prepared ferrite photocatalyst.

PACS numbers: 61.66.Fn, 81.05.Zx, 85.40.Zx
Keywords: Zinc ferrites, Nano-particles, Polymerized complex method, Visible light
DOI: 10.3938/jkps.55.1472

I. INTRODUCTION

In the present age of energy crises, we need to find an alternative renewable energy source *viz.* an efficient and eco-friendly solar hydrogen producing system. Simple perovskite metal oxides have been explored, which has led to several exciting and attractive developments in UV photocatalysis; however due to the abundance of solar energy, the development of visible-light photocatalysts has become an important issue in photocatalysis research today because the solar spectrum contains only ca. 4% UV light and ca. 46% visible light, indicating that low-band-gap catalysts are more desirable.

To date, many groups have developed active visible-light photocatalysts of various oxides, sulfides, oxynitrides *viz.* $PbBi_2Nb_2O_9$, $(Ga_{1-x}Zn_x)(N_{1-x}O_x)$, $Ni_xIn_{1-x}TaO_4$, TaON, $TiO_{2-x}N_x$, $TiO_{2-x}C_x$, and $Sm_2Ti_2O_5S_2$, *etc.* [1–8], but we still need a low-band-gap (ca. 1.9 ∼ 2.1 eV), high-efficiency photocatalyst so that the visible-light photons from the solar spectrum are efficiently utilized. An *n*-type $ZnFe_2O_4$ with a spinel structure is an attractive candidate for visible-light photocatalysis because it has a relatively small band-gap (ca. 1.9 eV), which is necessary to absorb a larger percentage of the visible light from the solar spectrum; thus making it a potentially useful solar energy conversion material.

Recently we observed that a photocatalyst consisting of nanocomposites was efficient in utilizing visible-light photons and in showing unprecedented high activity for the photocatalytic oxidation of water under visible-light irradiation ($\lambda \geq 420$ nm) [9–11]. Thus exploring the photocatalytic activity of a single component, a nanocrystalline ternary metal-oxide *i.e.* $ZnFe_2O_4$ is of prime importance and of particular interest for the development of an active visible-light, high-efficiency composite photocatalyst. In recent years, the polymerized complex

*E-mail: hhgkim@kbsi.re.kr

(PC) method has been widely used to prepare multiple-metal-containing oxides due to its uniqueness in yielding an improved crystallinity and homogeneity at low temperature for relatively smaller particle dimensions. In addition, such photocatalysts have shown an enhanced photocatalytic activity [12].

In this paper, we describe the synthesis of an *n*-type photocatalyst of $ZnFe_2O_4$ having a spinel structure, by using the PC method, and we report the physicochemical properties of the nanocrystalline $ZnFe_2O_4$, which were measured by using ultraviolet-visible (UV-VIS) diffuse reflectance spectroscopy (DRS), X-ray diffraction (XRD), and morphological studies. Further, we also report the photocatalytic and photoelectrochemical performance of the material for photocurrent generation and its photocatalytic ability under visible-light irradiation ($\lambda \geq 420$ nm). Surprisingly, the $ZnFe_2O_4$ made by PC method exhibits comparatively higher photocatalytic activity than the $TiO_{2-x}N_x$ [13].

II. EXPERIMENT

1. Preparation of Nanocrystalline $ZnFe_2O_4$

Nanocrystalline $ZnFe_2O_4$ was synthesiszed by using the PC method and a procedure similar to that described in our previous reports [14, 15]. Fig. 1 displays a schematic of the procedure used for synthesis of $ZnFe_2O_4$. Zinc nitrate hexahydrate ($Zn(NO_3)_2{\cdot}6H_2O$, 98.0%, Aldrich), ethylene glycol ($C_2H_6O_2$, Kanto Chemicals), citric acid ($C_6H_8O_7$, Wako), and iron nitrate hydrate ($Fe(NO_3)_3{\cdot}9H_2O$, 99.99%, Aldrich) were used as chemical precursors for the synthesis. The citric acid (CA) was added to water under constant agitation at a temperature of 60 – 70 °C. Further, the nitrate salts of zinc hexahydrate and iron hydrate were dissolved in the citric acid - water solution to obtain the metal-citrate complex. Finally, ethylene glycol (EG) was added to the mixture to yield a mass proportion of 60% CA to 40% EG. The mixture thus obtained was kept on a hot plate (80 °C) till it became a transparent colorless solution. The colorless solution was then heated at 130 °C for several hours to obtain a polymeric gel. The viscous polymeric product was pyrolyzed at about 300 – 500 °C to form the precursor powders. The powder thus obtained was pressed into the form of pellets, which were calcined at 500 – 1200 °C for 2 h in an electric furnace to obtain the nanocrystalline $ZnFe_2O_4$. In addition, $TiO_{2-x}N_x$ nanoparticles were also prepared using the hydrolytic synthesis method (HSM) [13] for the purpose of comparison. In this, an aqueous ammonium-hydroxide solution (an ammonia content of 28 – 30% (99.99%, Aldrich)) was slowly added drop by drop to a 20% titanium (III)-chloride solution ($TiCl_3$, Kanto, contained 0.01% iron as the major impurity) for 30 min under N_2 flow in an ice bath while continuously stirring the suspension for the next 5 h to complete the reaction. After the completion of the reaction, the precipitate was filtered in air and washed several times with deionized water. The filtered powder was dried at 70 °C for 3 – 4 h in a convection oven. The sample obtained at this stage was an amorphous precipitated powder containing traces of ammonia and titanium. Further, this sample was calcined at 400 °C for 2 h in air flow in an electric furnace to obtain crystalline powders of $TiO_{2-x}N_x$.

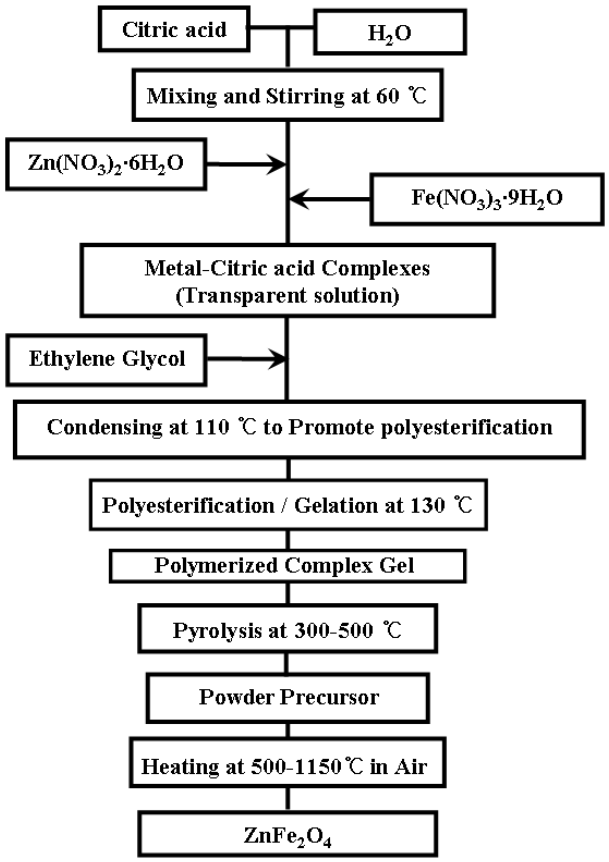

Fig. 1. A Flowchart for preparing $ZnFe_2O_4$ by using the polymerized complex method.

2. Characterization

The $ZnFe_2O_4$ samples were characterized by using X-ray diffractometer (Mac Science Co., M18XHF). The X-ray diffraction (XRD) results were compared with the Joint Committee Powder Diffraction Standards (JCPDS) data for phase identification. The band gap energy and the optical property of the as-prepared material were studied by using a UV-VIS diffuse reflectance spectrometer (Shimadzu, UV 2401). The morphology was determined by using a scanning electron microscopy (SEM, Hitachi, S-2460N) and high-resolution transmission electron microscopy (HR-TEM, Philips, CM 200). The Brunauer Emmett and Teller (BET) surface area

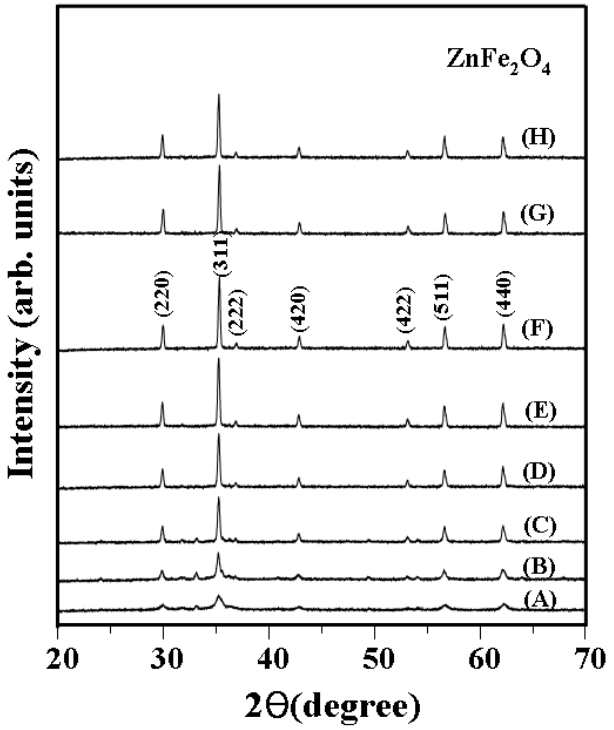

Fig. 2. XRD spectra of $ZnFe_2O_4$ samples prepared by using the polymer complex (PC) method and calcined at (A) 500 °C, (B) 600 °C, (C) 700 °C, (D) 800 °C, (E) 900 °C, (F) 1000 °C, (G) 1100 °C, and (H) 1200 °C for 4 h.

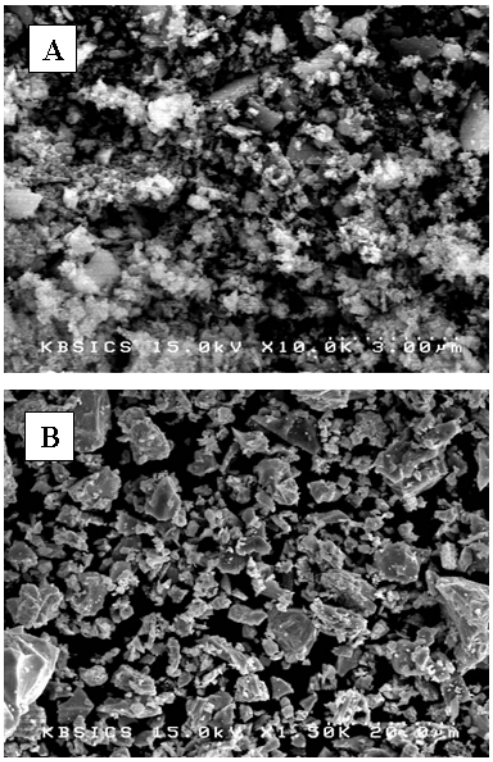

Fig. 3. SEM images of (A) $ZnFe_2O_4$, and (B) $TiO_{2-x}N_x$.

was estimated by using N_2 adsorption in a constant volume adsorption apparatus (Micrometrics, ASAP 2012).

3. Photocatalytic Reaction Procedure

The photocurrent generation and the photocatalytic water reduction/oxidation were studied for all samples under visible-light irradiation ($\lambda \geq 420$ nm). For the photoelectrochemical measurements [14], 25 mg of a photocatalyst was suspended in distilled water (75 mL) containing acetate (0.1 M) and Fe^{3+} (0.1 mM) as an electron donor and an acceptor, respectively, and the suspension pH was adjusted to 1.4 with $HClO_4$ to maintain the Fe^{3+} state. A Pt-plate ($10 \times 10 \times 0.125$ mm^3, both sides exposed to the solution), a saturated calomel electrode (SCE), and platinum gauze were immersed in the reactor as working (collector), reference, and counter electrodes, respectively. The photocurrents were measured by using a potentiostat (EG&G) to apply a potential (+0.6 V vs. SCE) to the Pt working electrode. These measurements were carried out under a N_2 purging atmosphere.

We estimated the hydrogen-producing activities from the half-reaction of water splitting during the photodecomposition of water in the presence of sacrificial agents. The rate of H_2 evolution was determined for the water-methanol solution (70 ml distilled water and 30 ml methanol) containing 0.1 g of catalyst. The concentration of H_2 was analyzed by using a gas chromatograph equipped with a thermal conductivity detector (molecular sieve 5-Å column and Ar carrier). The quantum yield (QY) was calculated as twice the number of generated H_2 molecules or four times the number of generated O_2 molecules divided by the number of photons absorbed by the photocatalyst. Before both reactions, 1 wt% of Pt was deposited on the photocatalysts, by using a photodeposition method, under visible light ($\lambda \geq 420$ nm).

III. RESULTS AND DISCUSSION

A structural characterization of these chemically synthesized samples was carried out to study the evolution of the required phase with respect to the variation in the calcination temperature. Fig. 2 displays the XRD patterns of the samples calcined at various temperatures, showing the peaks related to the $ZnFe_2O_4$ crystal structure. The formation of spinel the $ZnFe_2O_4$ structure, along with the other impurity phases, was observed in the samples calcined in range of 500 – 700 °C. The sample calcined in the range of 800 – 1200 °C exhibited a single phase of $ZnFe_2O_4$ without any impurity phase. This indicates that by using a chemical method, the $ZnFe_2O_4$ phase can be formed at a low temperature, yielding a pure phase at relatively lower temperatures [14,15].

Table 1. Observed band gap and hydrogen evolution values for 1 wt% Pt loaded materials in water-methanol mixtures.

Catalyst	Band gap energy		Hydrogen evolution	
	E(eV)	λ_{ab}(nm)	mmol/gcat.hr	QY(%)
$ZnFe_2O_4$	1.90	610	1.3	0.15
$TiO_{2-x}N_x$	2.73	451	Trace	0

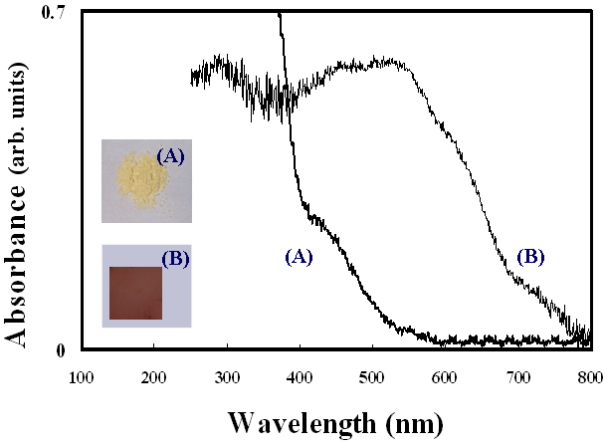

Fig. 4. UV-Vis diffuse reflectance spectra of (A) $TiO_{2-x}N_x$ and (B) $ZnFe_2O_4$ (1000 °C for 4 h). The inset the color of the as-synthesized samples.

Figure 3 compares the SEM images of (A) $ZnFe_2O_4$ and (B) $TiO_{2-x}N_x$ crystals. The samples consist of the fine particles of 3 – 10 μm in size. These particles consist of smaller nanocrystals of 53.0 nm, as estimated from Scherrer's analysis in Fig. 2 [16]. The particles of $TiO_{2-x}N_x$ were found to be larger in size than the ferrite particles.

UV-Vis diffuse reflectance spectra for the ferrite sample (calcined at 1000 °C) and the $TiO_{2-x}N_x$ sample are displayed in Fig. 4. We estimated the band gap energies of these materials, and they are given in Table 1. The $ZnFe_2O_4$ showed a sharp edge while $TiO_{2-x}N_x$ showed two absorption edges; a main edge due to the oxide at 390 nm and a shoulder due to the nitride at 451 nm [5]. The band gaps were found to be 1.90 eV and 2.76 eV, respectively, for $ZnFe_2O_4$ and $TiO_{2-x}N_x$. The dark brown and yellow colors of these materials also indicate that they absorb visible light, as desired for a visible-light photocatalyst.

Active visible-light photocatalysts should generate photocurrents upon absorption of photons. To investigate the photocurrent generation, we illuminated the aqueous suspensions of materials containing acetate (donor) and Fe^{3+} (acceptor) with visible-light ($\lambda \geq 420$ nm) photons. Fig. 5 shows the photocurrents generated by $ZnFe_2O_4$ and $TiO_{2-x}N_x$ samples. Unmodified TiO_2 with a wide band gap (3.2 eV) under irradiation, as well as other catalysts in the dark, did not generate any photocurrent, as expected. The ferrite sample

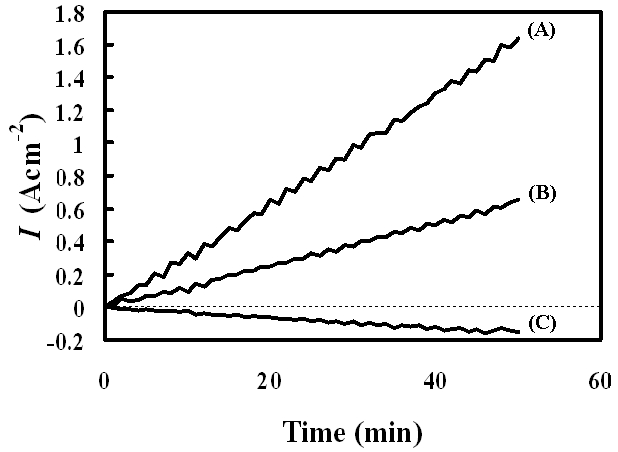

Fig. 5. Generated photocurrents under visible light ($\lambda \geq$ 420 nm) irradiation for $TiO_{2-x}N_x$ and $ZnFe_2O_4$ material suspensions with acetate and Fe^{3+} as an electron donor and acceptor, respectively; (A) $ZnFe_2O_4$ (1000 °C for 4 h); (B) $TiO_{2-x}N_x$ and (C) TiO_2 . Experimental conditions: photocatalysts = 0.025 g/75 ml; acetate = 0.1 M; Fe^{3+} = 0.1 mM; continuous N_2 purging; pH = 1.4; Eapp = 0.6 V (vs SCE); Pt plate (10 × 10 × 0.125 mm^3), Pt-gauze as working and counter electrodes, respectively.

calcined at 1000 °C generated a photocurrent approximately 15 times faster than the $TiO_{2-x}N_x$ sample did. The generation of a photocurrent is a critical initial step in photocatalytic reactions upon light irradiation, and the values of the current can be directly correlated with the photocatalytic activity of the photocatalyst.

We loaded platinum nanoparticles on all the samples prior to the photocatalytic studies. We used a photodeposition method [17,18] for this purpose. Fig. 6 shows HR-TEM images of 1 wt% platinum-loaded (A) $ZnFe_2O_4$ and (B) $TiO_{2-x}N_x$ samples. Both shows well-dispersed platinum (3 $\sim$ 4 nm) nanoparticles on the particle surface. The platinum nanoparticles were found to exhibit a uniform distribution over the particle surface in both cases.

We performed the photo-reduction reaction of water-methanol mixtures under visible light (≥420 nm). Fig. 7 shows the photocatalytic activity of ferrite, along with that of the oxynitride sample. The hydrogen production over the ferrite sample increased steadily with the reaction time, following this the photoreaction system was evacuated for 5 h in order to remove gaseous products from the gas phase, as shown in Fig. 7; thus, one can conclude that H_2 evolution over the photocatalysts occurred photocatalytically. The quantum yield (QY) for the photocatalysts of the material were calculated using the following the equation [19].

$$QY = H_2\text{evolution rate}/12.639 \times [(I_1 - I_3) - (I_1 - I_2)] \times A_1/A_2 \times 100, \quad (1)$$

where I_1 is the blank light intensity, I_2 is the scattered light intensity, I_3 is the photocatalyst light intensity, A_1

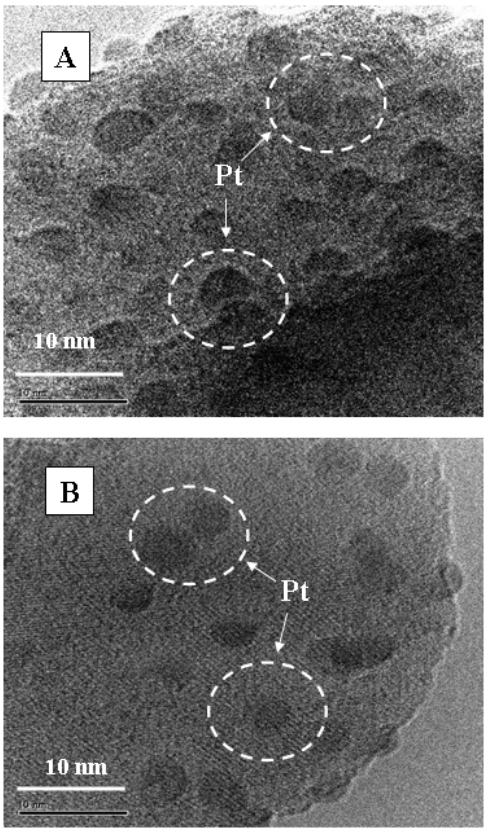

Fig. 6. HR-TEM images of a 1 wt% platinum-loaded (A) $ZnFe_2O_4$ (1100 °C for 4 h) and (B) $TiO_{2-x}N_x$. The Pt was deposited on the photocatalysts by using the photodeposition method under visible light ($\lambda \geq 420$ nm).

is the illuminated area of the photoreactor, A_2 is area of the sensor, and 12.639 is the mole number of photons with $\lambda \geq 420$ nm emitted from the lamp during 1 h. The estimated QYs of the $ZnFe_2O_4$ and the $TiO_{2-x}N_x$ samples were 0.15 and nil (trace amount), respectively.

Surprisingly, $ZnFe_2O_4$ had not been explored rigorously in the past for the photo-reduction of water though it showed a significant quantum yield compared to titanium oxynitride (see Table 1). In order to validate the observation, we carried out flat band potential measurements. Fig. 8 shows a schematic of the flatband potential for zinc ferrite and titanium oxynitride, as estimated from pH-dependent photocurrent measurements. We found that the top of the conduction band for zinc ferrite was very similar to that of the oxynitride, indicating that, like oxynitride, the ferrite photocatalyst is also suitable for hydrogen evolution from water-methanol mixture. The correlation between photocatalytic activity (Fig. 7) and photoelectrochemical response (Fig. 5) indicates the superiority of $ZnFe_2O_4$ over $TiO_{2-x}N_x$ is due to the efficient absorption of visible-light photons due its small band gap. Thus, nanocrystalline $ZnFe_2O_4$ can be considered as an active component of a composite photocatalyst. In the case of half-cell reactions, it

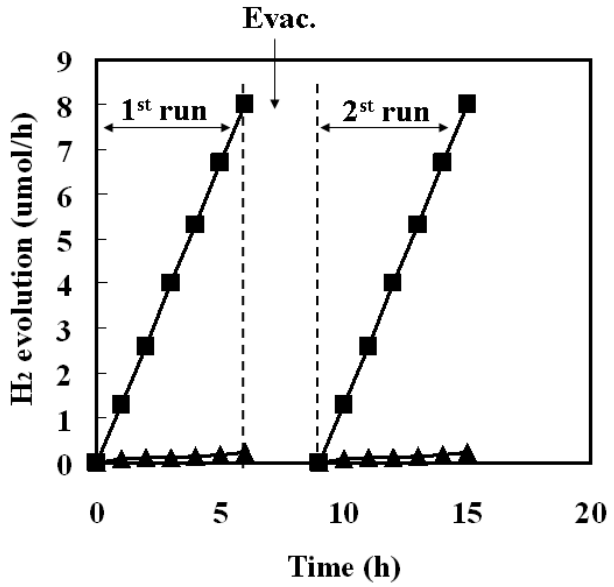

Fig. 7. Time course of H2 gas evolution from ■ $ZnFe_2O_4$ and ▲ N-Doped TiO_2 under visible light irradiation in an aqueous solution by stirring 0.1 g of catalyst loaded with Pt. The reaction system was evacuated every 5 h in order to remove gaseous products from the gas phase.

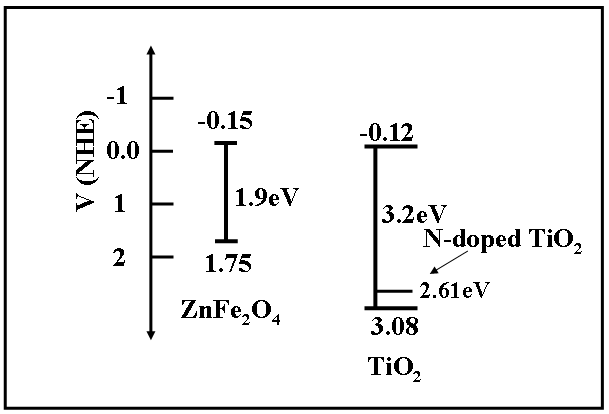

Fig. 8. The estimated electrochemical potentials (vs. NHE) for $ZnFe_2O_4$ and N-doped TiO_2 for band positions at pH =7, displayed along with the respective band gaps calculated from the pH-dependent photocurrent measurements.

can be considered for the decomposition of water under visible-light irradiation.

IV. CONCLUSIONS

A spinel-type zinc-ferrite material, $ZnFe_2O_4$, with high crystallinity, high surface area, and homogeneity has been successfully synthesized by using the polymer complex method. The visible-light induced hydrogen evolution from water-methanol mixtures with nanocrystalline $ZnFe_2O_4$ is much higher than that with $TiO_{2-x}N_x$.

Thus, nanocrystalline $ZnFe_2O_4$ with a spinel structure prepared by using the polymer complex method can be used as an efficient photocatalyst for half cell reaction under visible-light irradiation.

ACKNOWLEDGMENTS

This work has been supported by a Korean basic science institute (KBSI) grant T29320, MKE-RTI04-0201, Korean research foundation (KRF) grant (2005-042-C00174) and by the Hydrogen Energy R&D Center, Korea.

REFERENCES

[1] H. G. Kim, D. W. Hwang and J. S. Lee, J. Am. Chem. Soc. **126**, 8913 (2004).
[2] K. Maeda, T. Takata, M. Hara, N. Saito, Y. Inoue, H. Kobayashi and K. Domen, J. Am. Chem. Soc. **127**, 8286 (2005).
[3] Z. Zou, J. Ye, K. Sayama and H. Arakawa, Nature **424**, 625 (2002).
[4] G. Hitoki, T. Takata, J. Kondo, M. Hara, H. Kobayashi and K. Domen, Chem. Commun. 1698, (2002).
[5] R. Asahi, T. Ohwaki, K. Aoki and Y. Taga, Science **293**, 269 (2001).
[6] S. U. M. Khan, M. Al-Shahry and W. B. Ingler Jr., Science **297**, 2243 (2002).
[7] S. Sakthivel and H. Kisch, Angew. Chem. Int. Ed. **42**, 4908 (2003).
[8] A. Ishikawa, T. Takata, J. N. Kondo, M. Hara, H. Kobayashi and K. Domen, J. Am. Chem. Soc. **124**, 13547 (2002).
[9] H. G. Kim, P. H. Borse, W. Choi and J. S. Lee, Angew. Chem. Int. Ed. **44**, 4585 (2005).
[10] H. G. Kim, E. D. Jeong, P. H. Borse, S. Jeon, K. J. Yong, J. S. Lee, W. Li and S. H. Oh, Appl. Phys. Letts. **89**, 064103 (2006).
[11] S. J. Hong, P. H. Borse, S. M. Ji, J. S. Jang, J. S. Lee, E. D. Jeong, H. G. Kim and H. K. Pak, J. Korean Phys. Soc. **51**, S27 (2007).
[12] S. Ikeda, M. Hara, J. N. Kondo and K. Domen, Chem. Mater. **10**, 72 (1998).
[13] J. S. Jang, H. G. Kim, S. M. Ji, S. W. Bae, J. H. Jung, B. H. Shon and J. S. Lee, J. Solid State Chem. **179**, 1067 (2006).
[14] H. G. Kim, D. W. Hwang, S. W. Bae, J. H. Jung and J. S. Lee, Catal. Lett. **91**, 193 (2003).
[15] E. D. Jung, Pramod H. Borse, J. S. Jang, J. S. Lee, C. R. Cho, J. S. Bae, S. Park, O. S. Jung, S. M. Ryu and H. G. Kim, J. Nanosci. Nanotechnol. **9**, 3568 (2009).
[16] B. D. Cullity, *Elements of X-ray Diffraction*, 2nd ed. (Addison-Wesley Publishing Company, Inc., Reading, MA, 1978).
[17] J. Lee and W. Choi, J. Phys. Chem. B **109**, 7399 (2005).
[18] J. S. Jang, S. J. Hong, J. S. Lee, P. H. Borse, O. S. Jung, E. D. Jeong, T. E. Hong, M. S. Won and H. G. Kim, J. Korean Phys. Soc. **54**, 1 (2009).
[19] S. W. Bae, P. H. Borse, S. J. Hong, J. S. Jang, J. S. Lee, E. D. Jeong, T. E. Hong, J. H. Yoon, J. S. Jin and H. G. Kim, J. Korean Phys. Soc. **51**, S22 (2007).